BIOCHEMISTRY
including biophysical chemistry & molecular biology

Article

pubs.acs.org/biochemistry

A Nacre Protein, n16.3, Self-Assembles To Form Protein Oligomers That Dimensionally Limit and Organize Mineral Deposits

Iva Perovic,[†] Eric P. Chang,[†] Michael Lui,[†] Ashit Rao,[‡] Helmut Cölfen,[‡] and John Spencer Evans*[,†]

[†]Laboratory for Chemical Physics, Division of Basic Sciences and Craniofacial Biology, New York University, 345 East 24th Street, New York, New York 10010, United States

[‡]Department of Chemistry, Physical Chemistry, Universität Konstanz, Universitätstrasse 10, Konstanz D-78457, Germany

Supporting Information

ABSTRACT: The mollusk shell is a complex biological material that integrates mineral phases with organic macromolecular components such as proteins. The role of proteins in the formation of the nacre layer (aragonite mineral phase) is poorly understood, particularly with regard to the organization of mineral deposits within the protein extracellular matrix and the identification of which proteins are responsible for this task. We report new experiments that provide insight into the role of the framework nacre protein, n16.3 (*Pinctada fucata*), as an organizer or assembler of calcium carbonate mineral clusters. Using a combination of biophysical techniques, we find that recombinant n16.3 (r-n16.3) oligomerizes to form amorphous protein films and particles that possess regions of disorder and mobility. These supramolecular assemblies possess an intrinsically disordered C-terminal region (T64−W98) and reorganize in the presence of Ca^{2+} ions to form clustered protein oligomers. This Ca^{2+}-induced reorganization leads to alterations in the molecular environments of Trp residues, the majority of which reside in putative aggregation-prone cross-β strand regions. Potentiometric Ca^{2+} titrations reveal that r-n16.3 does not significantly affect the formation of prenucleation clusters in solution, and this suggests a role for this protein in postnucleation mineralization events. This is verified in subsequent *in vitro* mineralization assays in which r-n16.3 demonstrates its ability to form gel-like protein phases that organize and cluster nanometer-sized single-crystal calcite relative to protein-deficient controls. We conclude that the n16 nacre framework proteome creates a protein gel matrix that organizes and dimensionally limits mineral deposits. This process is highly relevant to the formation of ordered, nanometer-sized nacre tablets in the mollusk shell.

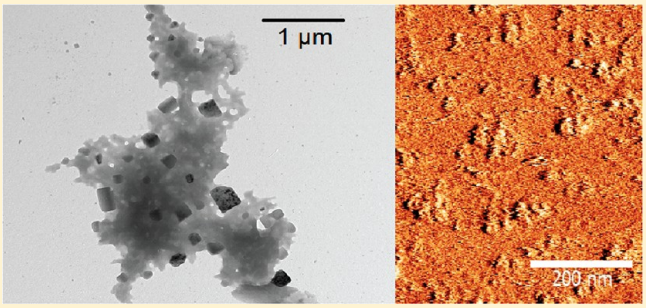

The biomineralization process in the mollusk shell is a complex bioengineering feat that leads to the formation of oriented, dimensionally controlled calcium carbonate mineral polymorphs of either calcite, aragonite, or both.[1−7] Important to this shell engineering process is the formation of the organic extracellular matrix (ECM), which oversees the mineralization process and tailors the formation of the prismatic (calcite) and/or nacre (aragonite) shell layers for the survival of each mollusk species.[8,9] To date, more than 50 different molluscan ECM protein genes have been identified, which indicates just how complex the shell formation process may be.[8−14] A subset of these proteins, known as the framework family,[5−8] are associated with the β-chitin polysaccharide−silk-like fibroin gel matrix[15,16] that coats the exterior of single-crystal aragonite tablets in the nacre layer of mollusks. It is known that this gel-like molecular matrix coating is an important medium for controlling calcium carbonate nucleation.[15−17] Hence, the framework proteome may be important for the formation of this gel phase and the subsequent mineralization events directed by this phase. Unfortunately, there is very little information available regarding the framework proteome and its participation in the nacre layer formation process. As a result, our present understanding of mollusk shell biomineralization is limited, and this in turn prevents us from developing promising materials science applications based upon the shell engineering process.

In the Japanese pearl oyster (*Pinctada fucata*), there exists a dominant group of framework proteins that are designated as the n16 proteome (n for nacre).[9,13,14,18,19] To date, 23 polymorphic forms of this family have been identified, and all of these forms are transcribed and actively expressed in the pearl oyster.[10,13] Interestingly, homologues of the n16 family have also been identified in the mollusks *Pinctada maxima* (N14 family)[11] and *Pinctada margaritifera* (Pmarg pearlin family).[9,12] This proteomic overlap suggests that n16-related sequences are an essential element in the construction of the nacre layer framework gel. With this in mind, attempts have been made to delineate the role of one member of this proteome, n16.3 (108 amino acids, 12947 Da).[17−19] This framework protein stabilizes aragonite *in vitro* in the presence of

Received: December 30, 2013
Revised: April 9, 2014
Published: April 10, 2014

   dx.doi.org/10.1021/bi401721z | *Biochemistry* 2014, 53, 2739−2748

Mg^{2+}[18] or as part of a protein complex with another *P. fucata* protein, Pif.[20] Intriguingly, the ability of n16.3 to stabilize aragonite without the presence of additives or other proteins is poor,[19] which suggests that this protein may perform other important roles with regard to nacre tablet formation. Structurally, the n16.3 protein is intrinsically disordered and consists of random coil and β turn sequences that are interspersed with amyloid-like extended β strand domains.[19,21] Under mineralization conditions, this interesting combination of sequence features endows n16.3 with self-associative properties that lead to the formation of heterogeneous protein oligomers.[19] Hence, n16.3 is an interesting representative of the *P. fucata* framework proteome, and understanding the structural−functional attributes of this protein in the oligomeric state will undoubtedly shed light on the *P. fucata* nacre formation process and related biomineralizing systems such as those found in *P. maxima* and *P. margaritifera*.[9,11,12]

At present, our knowledge of n16.3 is incomplete, especially with regard to the protein oligomerization process and the participation of these oligomers in specific scenarios within biogenic calcium carbonate nucleation and crystal growth processes.[22−25] To address these issues, we present a new study conducted with recombinant n16.3 (r-n16.3)[19] that not only provides additional information regarding framework protein oligomerization but also identifies an organizational function for framework proteins within the nacre mineralization scenario. We find that apo-r-n16.3 spontaneously forms amorphous films and oligomers that possess regions of backbone instability arising from the intrinsically disordered Gly, Asn rich C-terminal domain [positions 68−95 (Figure S1, Supporting Information)]. Interestingly, apo-r-n16.3 oligomers reorganize in the presence of Ca^{2+} to create clustered protein complexes, and this reorganization process alters the molecular environment of Trp residues in the protein. Using potentiometric titration methods,[22,25,26] we determine that r-n16.3 assemblies do not significantly affect the rate or quantity of prenucleation mineral clusters that form *in vitro*. However, via additional experiments, we were able to verify that r-n16.3 participates in the postnucleation phase of mineralization: the protein oligomers create a gel matrix that dimensionally limits and organizes mineral deposits and increases their solubility. Collectively, these processes are highly relevant to the formation of both the framework layer and the nacre tablets.

EXPERIMENTAL PROCEDURES

Recombinant Synthesis and Purification of r-n16.3. The gene synthesis, cloning, bacterial expression, and purification of r-n16.3 were performed by GenScript USA (Piscataway, NJ) using their proprietary OptimumGene system and recombinant expression systems as described elsewhere.[19] For heteronuclear nuclear magnetic resonance (NMR) experiments, uniformly labeled [U-^{13}C/^{15}N]r-n16.3 (hereafter termed CN-n16.3) was produced via recombinant bacterial overexpression in Bio-Express Cell Growth Media (U-^{13}C, 98%; U-^{15}N, 98%; Cambridge Isotope Laboratories, Andover, MA) by Genscript. The extent of double labeling was verified to be 98.9% using electrospray ionization mass spectrometry time of flight. For subsequent experimentation, r-n16.3 samples were created by exchanging and concentrating appropriate volumes of a stock solution into unbuffered deionized distilled water (UDDW) or other appropriate buffers using an Amicon Ultra 0.5, 3 kDa molecular mass cutoff apparatus (Millipore Corp.).

Mineralization Assays. Stock concentrations of r-n16.3 were prepared using unbuffered deionized distilled water. Mineralization assays were adapted from published protocols[27,28] and were conducted by mixing equal volumes of 20 mM $CaCl_2{\cdot}2H_2O$ (pH 5.5) and 20 mM $NaHCO_3/Na_2CO_3$ buffer (pH 9.75) until a final volume of 500 μL was reached in sealed polypropylene tubes and incubating the sample at room temperature for 1 min, 5 min, 15 min, and 1 h. Aliquots of the r-n16.3 stock solution were added to the calcium solution prior to the beginning of the reaction, with a final protein assay concentration of 10 or 25 μM, similar to that utilized in previous studies.[19] The final pH of the reaction mixture was measured and found to be approximately 8.0−8.2. Mineral and protein deposits formed during the assay were captured on either 5 mm × 5 mm Si wafer chips (Ted Pella, Inc.) or millimeter-sized freshly cleaved geologic calcite fragments (Iceland spar) that were placed at the bottoms of the vials. Upon completion of the mineralization assay period, the Si wafers and calcite fragments were rinsed thoroughly with calcium carbonate-saturated methanol and dried overnight at 37 °C prior to analysis. For transmission electron microscopy (TEM) studies, a 10 μL aliquot of the mineralization assay supernatant was withdrawn at the completion of the assay period, spotted onto Formvar-coated Au TEM grids (Ted Pella, Inc.), and then processed as described above.

Scanning Electron Microscopy. Imaging of the Si wafers extracted from the mineralization assays was performed using a Merlin (Carl Zeiss) field emission scanning electron microscope (FESEM) using either an Everhart-Thornley type secondary electron detector (SE2) or an annular secondary electron detector (in lens) at an accelerating voltage of 1.5 kV, a working distance of 4 mm, and a probe current of 300 pA. Prior to analysis, samples were coated with iridium using a Cressington 208HR sputter coater with a thickness controller attachment. X-ray microanalysis of the iridium-coated Si wafers was performed using an Oxford Instruments EDS with integrated INCA software attached to the Merlin FESEM. To perform the analysis, samples were lowered to a working distance of 8.0 mm and the acceleration voltage and probe current were increased to 2.0 kV and 1.2 nA, respectively. Areas of interest were scanned for 100 s each.

Transmission Electron Microscopy and Selected Area Electron Diffraction. Mineral and protein deposits that formed in mineralization assays were extracted from the mineralization reaction vials using 0.2 μm filtered calcium carbonate-saturated methanol and pipetted onto 200 square mesh gold grids coated with a Formvar carbon film (Electron Microscopy Sciences). TEM and electron diffraction were performed using a Philips CM12 transmission electron microscope equipped with a tungsten filament electron beam source. All imaging and diffraction analyses were performed at 120 keV. A diffraction pattern of a polycrystalline gold standard was used as a calibration scale for all subsequently recorded diffraction patterns. The selected area diffraction patterns were analyzed and indexed using ImageJ and the JEMS software package.

Potentiometric Ca^{2+} Titration. Potentiometric titration experiments were performed at room temperature by using a computer-controlled titration system operated with the supplied software (Tiamo version 2.2, Metrohm GmbH, Filderstadt, Germany). The experimental setup has been described previously.[22,26] A polymer-based ion-selective electrode and a flat-membrane glass electrode were used to monitor

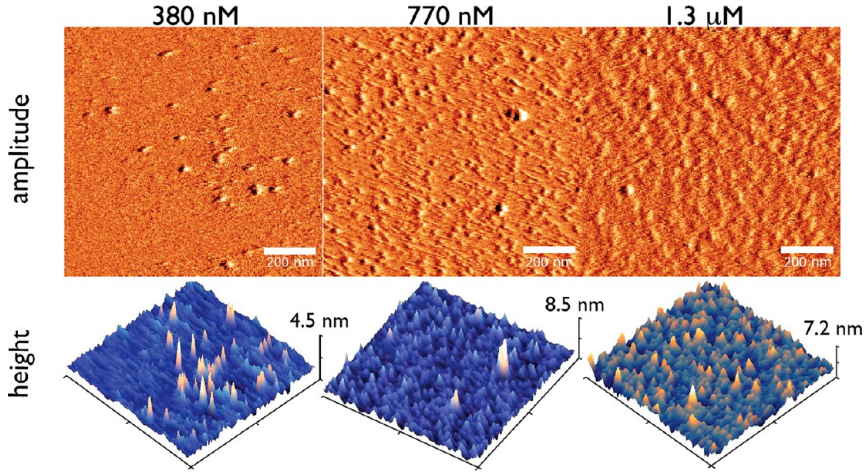

Figure 1. Concentration-dependent tapping mode AFM amplitude and height images of r-n16.3 on freshly cleaved mica surfaces at pH 8.0 and 10 mM Tris-HCl. All height plots are 1 μm × 1 μm in the x and y dimensions. Note in the height plots that the r-n16.3 oligomers form a contiguous filmlike layer or coating on the mica surface.

the free Ca^{2+} concentration and pH, respectively. During a titration run, a $CaCl_2$ (10 mM) solution was added at a constant rate of 0.01 mL/min to 10 mL of the protein solution in carbonate buffer (10 mM), which was constantly stirred at 800 rpm at room temperature. Parallel runs were conducted with 1.3 and 13.3 μM r-n16.3. A pH of 9.75 was maintained by countertitration of NaOH (10 mM). Reference and calibration experiments were performed by dosing $CaCl_2$ (10 mM) into carbonate buffer (10 mM, pH 9.75) and water (pH 9.75), respectively.

Atomic Force Microscopy (AFM) Imaging of r-n16.3 Assemblies. We investigated the dimensional and morphological characteristics of r-n16.3 assemblies captured from solution on mica substrates. AFM experiments[29] were executed at 25 °C using an Asylum MFP-3D stand-alone atomic force microscope operating in tapping mode in a buffer solution. V-Shaped Si_3N_4 cantilevers (reported spring constant of 0.09 N/m) were used for imaging. A precise drive frequency in fluid (~9 kHz) was calculated for each cantilever prior to imaging by overlaying the thermal spectrum over the frequency sweep. Several apo-r-n16.3 samples were imaged over a concentration range of 77 nM to 70 μM in 10 mM Tris-HCl (pH 8.0). A 1.3 μM apo-r-n16.3 sample was imaged in 10 mM $NaHCO_3$/Na_2CO_3 (pH 9.75). In addition, we also imaged a 77 nM r-n16.3 sample in 10 mM Tris-HCl and 12.5 mM $CaCl_2$ (pH 8.0). Note that imaging of Ca^{2+} samples utilized Tris-HCl as the buffering species instead of carbonate or bicarbonate, because carbonate ions will combine with Ca^{2+} ions and form inorganic precipitates that make protein complex detection and interpretation difficult to achieve via AFM. All samples were aliquoted onto a freshly stripped surface of mica (Ted Pella, Inc., 0.9 mm thick) and incubated for 15 min at ambient temperature prior to measurement. Igor Pro version 6.01 (http://www.wavemetrics.com) was used for image acquisition at a scan rate of 2 Hz. Gwyddion Software[30] was implemented for image processing, noise filtering, and analysis of surface parameters, such as R_q.

NMR Spectroscopy. A CN-n16.3 sample was created using lyophilized [U-^{13}C/^{15}N]r-n16.3 dissolved in 10 mM Tris-HCl and 10% (v/v) D_2O (99.99 atom % D, Cambridge Isotope Laboratories) in the absence of any buffer (i.e., the protein acts as its own buffer). The pH of this sample was adjusted with microliter volumes of 1 N NaOH to a final value of 7.5, and the final protein concentration was 70 μM in a volume of 300 μL. Note that base-catalyzed amide backbone exchange kinetics at pH ≥8.0 prevents the collection of interpretable NMR data for CN-n16.3 under mineralization conditions. Thus, we performed experiments at pH 7.5, which is close to this pH range and allows for maximal detection of exchangeable backbone and side chain N−H spin systems. Note also that the 70 μM r-n16.3 sample at pH 7.5 forms large protein assemblies similar to those obtained at pH 8.0 (Figure S2, Supporting Information). Samples were placed in 5 mm symmetrical D_2O-matched Shigemi NMR microtubes (Shigemi, Inc., Alison Park, PA). No visible aggregation was evident, and periodic ^{15}N heteronuclear single quantum coherence spectroscopy (HSQC) experiments were conducted to verify that line width broadening or chemical shift changes associated with aggregation did not occur. NMR data of CN-n16.3 were collected at 25 °C using a Bruker AVANCE 900 MHz spectrometer equipped with a four-channel 5 mm cryoprobe. The operating Larmor frequencies were 900.26 MHz for proton, 125.76 MHz for carbon, and 91.22 MHz for nitrogen. Bruker TOPSPIN was used to process all data. The spectra were referenced with respect to the temperature-corrected water resonance, and ^{15}N chemical shifts were referenced on the basis of the ^{1}H IUPAC guidelines using the unified chemical shift scale.[31]

Fluorescence Spectroscopy. The intrinsic tryptophan fluorescence emission of apo-r-n16.3 as a function of protein concentration (77 nM, 386 nM, 772 nM, or 1.3 μM) in the presence of Ca^{2+} [1.3 μM r-n16.3, with r-n16.3:Ca^{2+} stoichiometries of 0, 1:1, 1:10, 1:20, and 1:9615 (or 12.5 mM $CaCl_2$)] was obtained using a Hitachi F2500 fluorescence spectrometer at 25 °C, with the excitation and emission slit widths set at 5 and 10 nm, respectively. The protein samples were excited at 280 nm, and their characteristic emissions were monitored between 290 and 500 nm, with an average of three scans per sample. The scatter contributions were removed by subtracting the appropriate blank spectrum from every measurement.[32−34]

dx.doi.org/10.1021/bi401721z | *Biochemistry* 2014, 53, 2739−2748

RESULTS

In previous bioinformatics studies, we identified the location of intrinsically disordered and amyloid-like aggregation-prone domains in n16.3 (Figure S1, Supporting Information) and found that these two traits are shared by the majority of documented nacre protein sequences.[21] In n16.3, the most significant intrinsically disordered sequence is a 27-amino acid repetitive Gly, Asn region (i.e., the -NG- motif, positions 68–95) located in the C-terminal region of the protein. Four putative cross-β strand regions were identified,[21] and upon re-examination of that data set, we discovered that four of the five Trp residues (W13, W37, W40, and W50) are located within a predicted cross-β strand region. As we shall see below, these Trp residues may play a role in some aspect of n16.3 oligomerization.

r-n16.3 Spontaneously Forms Films and Oligomeric Complexes. Previously, the self-association of r-n16.3 was studied as a function of pH and Ca^{2+} concentration using dynamic light scattering (DLS).[19] Understandably, these studies required the use of filtration, and thus any >0.2 μm protein oligomers, not to mention protein films, would have evaded analyses. To probe beyond this limit, we utilized tapping mode AFM imaging on freshly cleaved mica surfaces to more precisely monitor r-n16.3 oligomerization under relevant conditions (i.e., pH 8 of *in vitro* mineralization assays).[19,29] Here, we observe the formation of nanometer-sized oligomers over a wide range of r-n16.3 concentrations (Figure 1). In general, these oligomer are amorphous in appearance and heterogeneous in dimension as evidenced by quantitative measurements extracted from the AFM images (Table 1).

Table 1. r-n16.3 Protein Oligomer and Surface Roughness (R_q) Parameters Determined by Tapping Mode AFM under Various Solution Conditions[a]

sample	average oligomer height (nm)	average oligomer diameter (nm)	R_q (nm)
fresh mica	–	–	0.1
apo, 77 nM	2.9 ± 1.3	30 ± 9	0.22
apo, 386 nM	4.2 ± 2.0	34 ± 5	0.59
apo, 770 nM	3.3 ± 1.1	50.2 ± 14.1	0.9
apo, 1.3 μM	2.8 ± 0.7	49.8 ± 21.1	0.54
apo, 77 nM	2.9 ± 1.3	30 ± 9	0.22
12.5 mM Ca^{2+}, 77 nM	1.5 ± 0.4	27 ± 15	0.27

[a]All samples were measured in 10 mM Tris-HCl buffer (pH 8), except as noted. Using line profile extraction of amplitude and height images of 50 representative oligomers, we calculated the average oligomer heights, diameters, and root-mean-square surface roughnesses (R_q) for these protein samples.

Furthermore, the contrast between surface roughness values (R_q) for the freshly cleaved mica surface in buffer (R_q = 0.078 nm) and untreated mica surfaces exposed to apo-r-n16.3 (R_q = 0.22–0.28 nm, an approximately 3–3.5-fold increase) confirms that r-n16.3 forms protein films on mica surfaces, consistent with previous reports of the formation of protein films on Si supports.[19] From this, we conclude that the r-n16.3 supramolecular assemblies exist as a two-component system of films and protein oligomers that are structurally amorphous.

Apo-r-n16.3 Oligomers Possess Labile, Disordered Protein Domains. From previous NMR studies, we know that biomineralization protein assemblies exhibit very few multi-dimensional NMR cross-peaks.[32,35–37] This is particularly true for residues that are involved in intermolecular contacts, because protein–protein interactions lead to changes in backbone dynamics and intermediate time scale broadening, and as a consequence, signal intensity attenuation occurs for nearly all NMR resonances. However, for supramolecular complexes formed by intrinsically disordered proteins, there are a number of NMR resonances that are not attenuated in this fashion and hence can be observed via TOCSY, HSQC, or other experiments.[32,35–37] These detectable spins are the result of permissible protein backbone motions originating from either disordered or residually structured regions that are not restrained by intermolecular contacts. Thus, solution NMR experiments can provide evidence of (and in some case the location of) disordered or unrestrained domains within protein assemblies.

Using ^{15}N-edited HSQC experiments, we find that r-n16.3 oligomers [70 μM CN-n16.3 (pH 7.5) (Figure S2, Supporting Information)] exhibit the characteristic molecular signature of disordered protein assemblies (Figure 2). As expected,

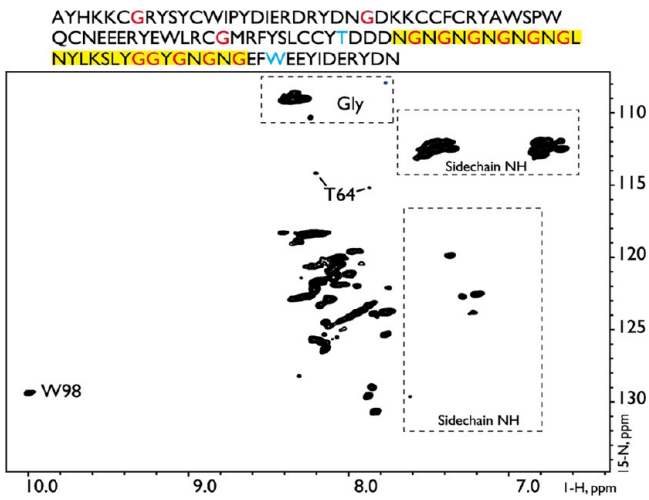

Figure 2. ^{1}H–^{15}N HSQC NMR spectrum of 70 μM CN-n16.3 in 10 mM Tris (pH 7.5). Tentative assignments of side chain and backbone spin systems are shown. For comparison, we present the primary amino acid sequence of n16.3, highlighting the location of Gly residues (red), the Gly, Asn repeat region (yellow highlighting), and Thr and Trp residues (blue) that reside in the proximity of the Gly, Asn repeat.

intermolecular contacts between protein molecules lead to the attenuation of the majority of backbone HSQC resonances for this sample (Figure 2). However, we were able to detect a limited number of ^{1}H, ^{15}N backbone and side chain resonances originating from r-n16.3 assemblies, and thus, a population of unrestrained sequence regions exist within these oligomers. Although complete sequential assignments are not feasible for these protein assemblies, fortunately the n16.3 sequence contains a significant content of Gly (14 amino acids) and Trp (five amino acids) and a single Thr (T64). These three amino acids give rise to backbone and/or side chain ^{1}H, ^{15}N chemical shift distributions that are easily distinguishable from those of other amino acid resonances. Using this approach, we analyzed the HSQC spectra for these unique ^{1}H, ^{15}N chemical shifts and identified the presence of NMR cross-peaks arising from several Gly residues, a single Trp, and the single Thr [i.e., T64 (Figure 2)]. We note that most Gly residues reside within the repetitive -NG- sequence domain near the C-terminal end

dx.doi.org/10.1021/bi401721z | *Biochemistry* 2014, 53, 2739–2748

of the protein (sequence positions 68−95). Given that Gly and Asn are known sequence disorder promoters,[38−41] we tentatively assigned the ^{1}H, ^{15}N HSQC Gly α, α' cross-peaks to this repeat sequence. This Gly assignment was also supported by the NMR data obtained for T64 (Figure 2). Here, we found two HSQC cross-peaks that can be assigned to T64. When multiple NH cross-peaks do exist for a given residue, it is usually indicative of backbone chemical or conformational change processes.[32,34−37] The identification of a T64 species undergoing conformational exchange is significant in that the T64 is positioned immediately upstream of the disordered -NG- sequence domain. Thus, if T64 is undergoing conformational exchange, then it must be in response to a nearby destabilized or labile sequence region such as the -NG- repeat. Hence, the observed Gly NMR cross-peaks are most likely associated with this repeat region. Given the -NG- induction effect on T64, it was then logical to assume that the single Trp NMR indole ring resonance (Figure 2) must also be associated with this disordered repeat sequence, as well. It turns out that only one Trp residue (W98) resides near the disordered -NG- domain (Figure 2), and thus, we assigned this cross-peak to W98. In conclusion, our heteronuclear NMR experiments verified the presence of an intrinsically disordered or unrestrained T64−W98 sequence region within assembled r-n16.3 protein molecules. Note that it is possible that other disordered regions also exist within r-n16.3 oligomeric assemblies, but these cannot be assigned at present.

Ca^{2+} Induces Clustering of r-n16.3 Complexes. In previous r-n16.3 DLS studies, it was noted that protein particle hydrodynamic radii increased in response to Ca^{2+}.[19] To more accurately determine what effect this cation has on protein oligomerization and oligomer morphology, we revisited the Ca^{2+} scenario again using AFM tapping mode imaging.[21] Given the potential for the involvement of Trp in the oligomerization and/or oligomer stabilization (Figure S1, Supporting Information),[32] we performed fluorescence spectroscopy experiments to probe any changes in intrinsic Trp fluorescence emission[32−34] in the presence and absence of Ca^{2+} and thus monitor perturbations in the Trp molecular environment as we go from the apo state to conditions that approximate the mineralization assay state.

As shown in Figure 3, relative to the apo state we observe that Ca^{2+} induces clustering of protein oligomers at low protein concentrations (i.e., 77 nM), yet the particle dimensions and R_q values for both scenarios remain relatively constant compared to those of the apo state (Table 1). Thus, this clustering effect on mica surfaces is largely a two-dimensional phenomenon. If one progresses to higher protein concentrations (i.e., micromolar), then the overall z thicknesses of Ca^{2+}-treated r-n16.3 oligomers increase significantly and interfere with AFM tip positioning (data not shown). For this reason, we were unable to obtain reliable images of r-n16.3 particles and films in the presence of Ca^{2+} beyond the 77 nM protein range. Nonetheless, at low protein concentrations, we confirm that Ca^{2+} promotes further aggregation or clustering of protein oligomers relative to the apo state.

Because the intrinsic fluorescence emission of tryptophan is sensitive to the environmental polarity and proximity of other residues,[32−34] we exploited this property to investigate the assembly of r-n16.3 and the impact of Ca^{2+} on protein oligomerization. In the apo state, r-n16.3 oligomers exhibit a λ_{max} of 344 nm in Tris-HCl buffer (pH 8.0) (Figure 3). As Ca^{2+} concentrations approach those utilized in mineralization assays,

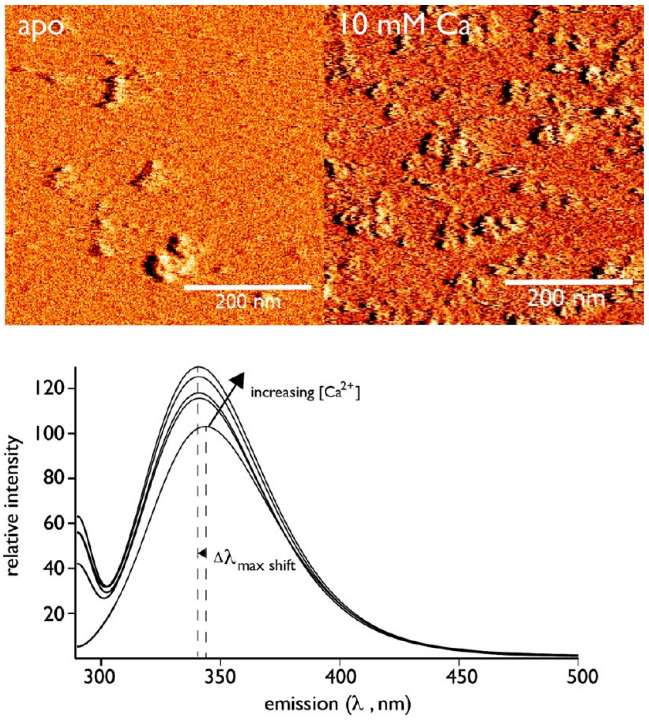

Figure 3. Tapping mode AFM amplitude images of 77 μM r-n16.3 with 10 mM Tris-HCl (pH 8.0) on freshly cleaved mica surfaces in the apo state and in the presence of 12.5 mM $CaCl_2$. Accompanying these images are Trp fluorescence emission spectra of 1.3 μM r-n16.3 in the apo state and in the presence of Ca^{2+} with r-n16.3:Ca^{2+} stoichiometries of 0, 1:5, 1:10, 1:20, and 1:9615 (or 12.5 mM $CaCl_2$ utilized in previously published mineralization assays). Increasing r-n16.3:Ca^{2+} ratios are indicated by the arrow. Dashed vertical lines define the $\Delta\lambda_{max}$ for the apo and 12.5 mM $CaCl_2$-loaded r-n16.3 samples. Raw data were smoothed using a binomial algorithm with bounce end effects.

we observe two trends in the intrinsic fluorescence signature for Trp: an enhancement of the emission fluorescence maximal intensity (13−22%) and a small blue shift ($\Delta\lambda_{max}$ = 2−6 nm) in the emission wavelength relative to that of the apo state at pH 8.0. Typically, Trp residues in proteins exhibit blue shifts in their emission profiles as the local environment undergoes a transition from a hydrophilic to a hydrophobic and less solvent-accessible nature.[32−34] Thus, our results indicate that Trp residues are undergoing a transition toward a more shielded or hydrophobic environment in response to Ca^{2+}-induced oligomer reorganization or cluster formation (Figure 3). Given that four of five Trp residues reside in putative cross-β strand aggregation-prone regions within r-n16.3 (Figure S1, Supporting Information),[21] we conclude that Ca^{2+}-induced r-n16.3 oligomeric reorganization or clustering processes involve these regions.

r-n16.3 Assemblies Have a Minimal Effect on Prenucleation Cluster Formation and Kinetics. It is known that biological calcium carbonate mineralization utilizes a nonclassical nucleation scheme that involves the initial formation of nanometer-sized prenucleation clusters (PNCs) that assemble into larger clusters of amorphous calcium carbonate (ACC).[22−26] With that in mind, we wished to address the potential role that nacre protein assemblies, such as those generated by n16.3, might play in a nonclassical nucleation process. To do this, we performed potentiometric calcium titrations of r-n16.3 alongside reference experiments (i.e., protein-deficient) (Figure 4 and Table 2). Note that r-

dx.doi.org/10.1021/bi401721z | Biochemistry 2014, 53, 2739−2748

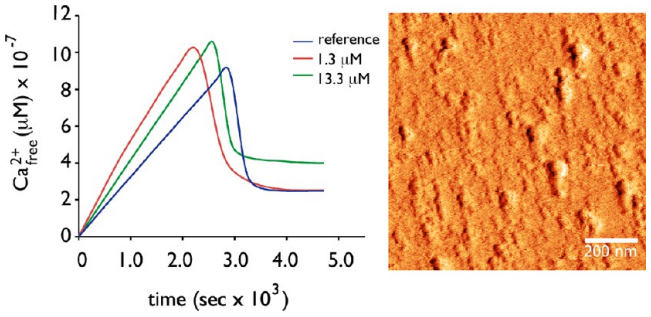

Figure 4. Potentiometric Ca^{2+} titration of 1.3 and 13.3 μM r-n16.3 in 10 mM Na_2CO_3 (pH 9.75) as a function of time. The reference curve refers to parallel experiments conducted in the absence of protein. Alongside the potentiometric plot is a tapping mode AFM amplitude image obtained for a 1.3 μM r-n16.3 sample in 10 mM $NaHCO_3$/Na_2CO_3 (pH 9.75) on a freshly cleaved mica surface. Note that this AFM image is qualitatively similar to the image obtained for 1.3 μM apo-r-n16.3 at pH 8.0 (Figure 1).

Table 2. Calcium Potentiometric Titration Data Obtained for r-n16.3 Protein Oligomers and Reference (protein-deficient) Samples

sample	nucleation time (s)	prenucleation slope (mol/s^2)	solubility (M^2)[a]
reference	2898	3.2×10^{-10}	3.4×10^{-8}
1.3 μM	2275	4.6×10^{-10}	2.6×10^{-8}
13.3 μM	2580	4.2×10^{-10}	5.4×10^{-8}

[a]Postnucleation solubility.

n16.3 oligomerization is significant at pH 9.75 as evidenced by the presence of protein films and large oligomer particles (Figure 4, 1.3 μM sample). With regard to PNC formation, we note that the time intervals when nucleation and ripening occur are slightly altered (within 10%) by r-n16.3 relative to the control scenario (Figure 4 and Table 2). These differences have been shown to be attributable to experimental deviations and are minor compared to the reported nucleation inhibition observed for synthetic polyelectrolyte additives.[25,26,42] Thus, r-n16.3 does not significantly accelerate or delay the nucleation and ripening processes and has little effect on the induction time for PNC formation.

We also utilized these same potentiometric experiments to determine postnucleation solubility (Table 2 and Figure S3, Supporting Information). Here, we observe changes in mineral solubility that are protein concentration-dependent. In the reference experiments, the solubility product of the initial phase formed after nucleation was 3.6×10^{-8} M^2. This is consistent with previous reports and indicates the formation of vateritic ACC at pH 9.75.[25,26,42] At 1.3 μM r-n16.3, the postnucleation solubility product decreases relative to the reference state yet still indicates the formation of an ACC mineral phase (Table 2). However, at 13.3 μM r-n16.3, an increase in the ion solubility product occurs, and this suggests the formation of an alternate, more soluble ACC mineral phase.[25,26,42] On the basis of these findings, we conclude that r-n16.3 oligomers have an impact on postnucleation events that affect the solubility of the ACC phase.

r-n16.3 Protein Complexes Assemble Single-Crystal Nanodeposits into Clusters. In previous r-n16.3 *in vitro* mineralization studies, we observed the formation of single-crystal aragonite (<10% of the total crystals formed) as well as calcite and vaterite over a 16 h period (ammonium carbonate vapor diffusion, slow kinetics, pH 8.0).[19] However, these assays lacked precise control over carbonate content, which limits the reproducibility, and the need for assay time scales in excess of

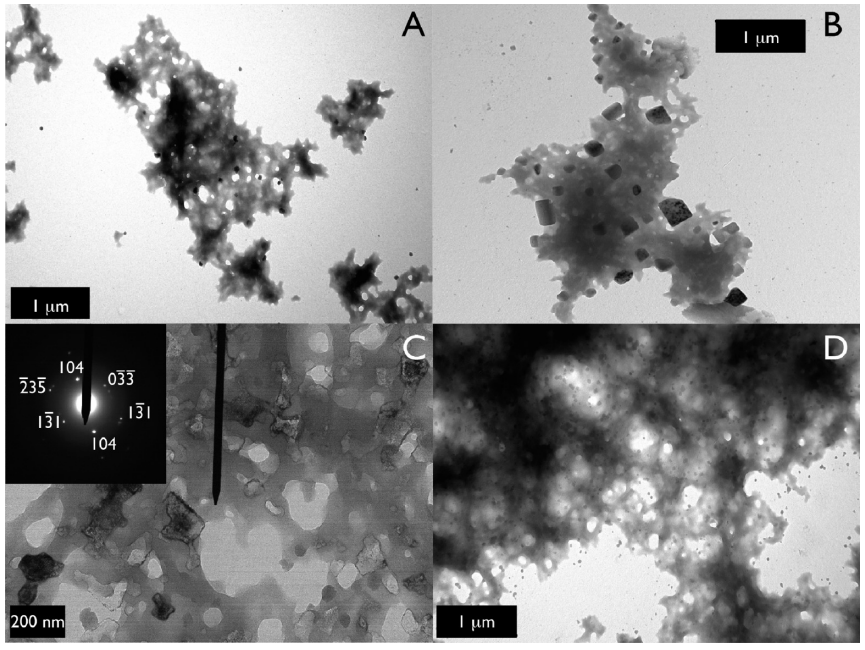

Figure 5. TEM images of total mineral and protein phases rescued at (A) 1 min, (B and C) 5 min, and (D) 15 min intervals from 10 μM r-n16.3 (pH 8.0) carbonate/bicarbonate mineralization assay experiments. Note the presence of small electron-dense particles within the protein phases in panels A and D. Image C is a higher-magnification image of a representative 5 min r-n16.3−mineral deposit complex or phase, with the corresponding electron diffraction pattern that indexes to single-crystal calcite. Note that spot or ring diffraction patterns could not be obtained for the 1 and 15 min samples. Other images of protein phases that were rescued from 5 min assays can be found in Figure S4 of the Supporting Information.

dx.doi.org/10.1021/bi401721z | *Biochemistry* 2014, 53, 2739−2748

10 h prevents direct assessment of early events in calcium carbonate nucleation that overlap with spontaneous protein oligomerization. To resolve this, we employed *in vitro* mineralization assays with defined bicarbonate/carbonate content (pH 8.0), a fixed protein concentration (10 μM), and shorter assay periods (1−15 min).[27,28] This allows us to concurrently track the spontaneous formation of r-n16.3 assemblies alongside the nucleation of calcium carbonates.

We first examined deposits that were rescued from assay supernatants as a function of time [1, 5, and 15 min (Figure 5)]. At 1 min, we detected r-n16.3 oligomeric films or deposits that appear to be gel-like and are associated with electron-dense nanometer-sized irregularly shaped deposits. These dense deposits, which do not give rise to detectable electron diffraction patterns, appear to be either entrapped within the protein films or surface-associated, similar to those noted for the intracrystalline mollusk nacre protein, AP7.[43] At 5 min, similar protein gel phases are present, but now the electron-dense deposits appear to be larger and can be identified as single-crystal calcite (Figure 5). What is distinctive about these 5 min protein−mineral complexes is the organization or clustering of the single-crystal calcite within the protein phase (Figure S4, Supporting Information). At 15 min, the protein phases are now considerably larger and denser, presumably as a result of Ca^{2+}-induced clustering of r-n16.3 oligomers (Figure 3). One can still discern nanometer-sized electron-dense deposits trapped inside these protein phases, and because of dimensional issues or interference from the protein phase, these mineral deposits do not give rise to interpretable electron diffraction patterns. If we compare the results obtained at 5 and 15 min, then we see that the characteristic protein-embedded calcite crystals at 5 min can no longer be discerned at 15 min. The absence of these single crystals is intriguing and may be attributable to one or more of the following phenomena. (a) At 15 min, the increased thickness of the protein phase now obscures the location of these crystals. (b) As the size of the crystals increases, the protein phase can no longer support them and the crystals separate from the film and elude capture by 15 min. (c) Some form of Ostwald ripening[22−26] is taking place between 5 and 15 min in our assay systems and may be linked to the postnucleation solubility increases induced by r-n16.3 complexes in solution (Table 2 and Figure S3, Supporting Information).

This scenario of r-n16.3 oligomer-mediated mineral cluster formation and dimensional control was also observed in our geological calcite assays (Figure 6).[29,44] These 1 h assays use the same solution conditions but utilize freshly cleaved geologic calcite fragments, both as a "capture" surface for forming mineral deposits in solution[29] and as a mineralization surface whose morphological features are susceptible to protein-induced modifications.[44] Relative to protein-deficient controls, we could find no evidence that r-n16.3 modified the morphology of the geologic calcite fragment surface relative to control conditions. Note also that we did not observe direct evidence of r-n16.3 films or phases collecting on the calcite surfaces; presumably, these are still present in the supernatant (Figure 5) and do not settle out or collect on the geologic calcite surfaces at 1 h. However, with regard to the captured calcite crystals, two interesting trends were noted. First, we find that the r-n16.3 assays feature captured calcite crystals that are dimensionally smaller than those found in the control assays (Figure 6). Second, the captured calcite crystals in the r-n16.3 assays appear to be clustered together (Figure 6), a phenomenon not observed in the control scenario. Because of the positioning of these crystal clusters on the geologic calcite surfaces, we were unable to directly visualize the presence of r-n16.3 phases that may have associated with these crystals. It is plausible that any associated film may be obscured by the clustered crystals themselves or may have separated from the crystals during SEM sample preparations. Nonetheless, using two different approaches, we confirm that r-n16.3 dimensionally limits crystal growth and functions as a mineral organizer or clustering agent.

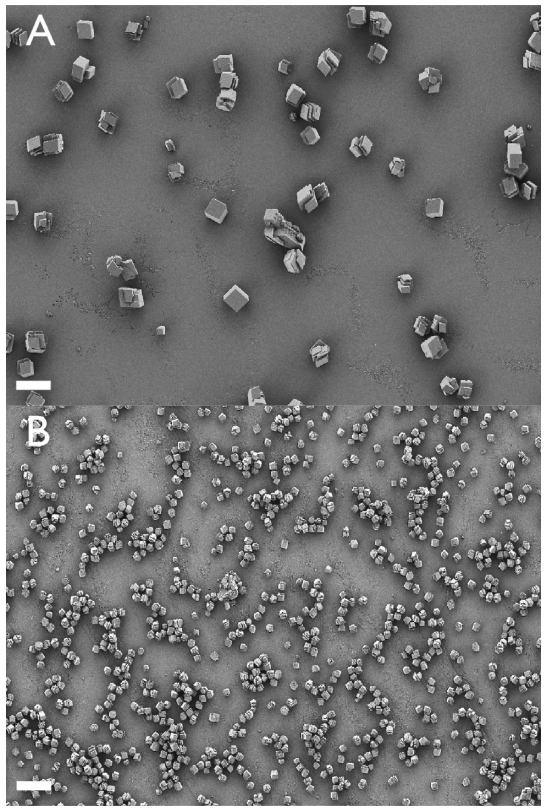

Figure 6. SEM images of mineral deposits formed on freshly cleaved geologic calcite {104} interfaces in (A) protein-deficient and (B) 25 μM r-n16.3-containing assays. The scale bar in each image corresponds to 10 μm.

DISCUSSION

The formation of aragonite tablets in the mollusk shell nacre layer requires organization of nucleation events, such that parallel-arranged single-crystal aragonite is produced in three dimensions.[5,6,15,16,45] This study represents the first attempt to map out the involvement of a nacre proteome within the nonclassical nucleation pathway for calcium carbonates and the architectural process of nacre tablet assembly. We present evidence that a single framework protein, r-n16.3, does not directly participate in the PNC formation process or significantly alter the kinetics of ACC formation (Figure 4).[22−26] Rather, this protein is involved in postnucleation events leading to the formation of nanometer-sized, organized single-crystal calcite (Figure 5). The ability of r-n16.3 to organize or assemble mineral particles is linked to the spontaneous self-assembly of this protein (Figure 1), and we note that these oligomers further cluster together in the presence of Ca^{2+} (Figure 3) and in mineral assays (Figure 5) to form protein phases. Thus, the formation of mineral-containing

protein phases (Figure 5 and Figure S4, Supporting Information) results from multiple mineral-containing protein oligomers clustering together over time (Figure 3). We believe that this activity would be critical in the protein-mediated formation of organized, dimensionally limited aragonite tablets in the nacre layer of the mollusk shell.[2,4−6,15,16,45] Given the sequence overlap within the n16 proteome and with the N14 and pearlin sequences,[8−14] it is likely that these homologous framework nacre protein families share similar functional mineralization traits and oligomeric properties that are associated with n16.3 (Figures 1−6).

Although we have documented the mineral organization capabilities of n16.3 in this study, we were unable to address aragonite formation and/or stabilization by this protein, which we originally reported on in earlier studies involving long-term ammonium carbonate vapor diffusion assays.[19] We believe that the absence of aragonite formation in this study is most likely due to the following: (a) the choice of mineralization assay conditions, which may favor calcite polymorph formation over aragonite in short-duration experiments;[25−28] (b) the omission of aragonite-promoting agents, such as Mg(II),[18] or small metabolites,[46] which may be necessary for efficient aragonite formation; and (c) aragonite stabilization activity represents a minor *in vitro* function of the n16.3 protein, as evidenced by the low efficiency (<10%) of aragonite formation generated by this protein in long-term diffusion assays.[19] We believe that all three factors are at play in our current experiments, and we intend to follow up on these initial findings with additional experiments that probe *in vitro* aragonite formation in the presence of r-n16.3 with additional agents.

This study also provides new observations regarding the molecular "disorganization" of n16.3 protein complexes. Previous circular dichroism experiments indicated that the protein molecules in r-n16.3 assemblies possessed random coil conformations in equilibria with other secondary structures such as extended β strand and β turn.[19] Using NMR spectroscopy, we extend these CD results and identify the C-terminal -NG- repeat (positions 64−98) as a major disordered region within r-n16.3 (Figure 2). Given the importance of intrinsically disordered regions to protein function,[38−41] we believe that this disordered region could play several important roles in r-n16.3 function: (a) maintaining r-n16.3 complexes in an amorphous, heterogeneous phase or state (Figure 1); (b) allowing r-n16.3 oligomers to undergo the transition between particle and filmlike morphologies (Figure 1 and Table 1) or reorganize into Ca^{2+}-clustered oligomeric phases (Figure 3); and (c) facilitating the assembly or retention of mineral deposits within the oligomers (Figure 5). The finding that r-n16.3 oligomers have persistent disordered regions has important consequences when one considers that more than 30 aragonite-associated proteins possess one or more intrinsically disordered sequence regions.[21] It may be that unfolded domains, such as the -NG- repeat, are important for nacre protein functionalities related to protein phases or mineralization. Additional studies will be essential in determining the identity and role(s) of intrinsically disordered sequences within the aragonite proteome.

At present, the role of tryptophan in biomineralization protein structure and function is not fully known. However, recent studies involving the formation of supramolecular complexes by the intrinsically disordered, aggregation-prone tooth enamel protein, amelogenin, demonstrated that specific Trp residues played an important role in the protein self-assembly process.[47,48] Our current study now provides evidence that Trp residues are functionally significant for the n16 framework nacre proteome. First, we note that W13, W37, W40, and W50 reside in putative cross-β strand aggregation-prone motifs (Figure S1, Supporting Information).[21] We were able to detect W98 in our HSCQ experiments, but the W13, W37, W40, and W50 resonances were attenuated (Figure 2). Thus, we believe that W13, W37, W40, and W50 are participants in r-n16.3 oligomer intermolecular interactions (Figure 2). Second, we find that Trp molecular environments are perturbed in the Ca^{2+}-induced oligomer reorganization process (Figure 3), and this result suggests two possible scenarios. (a) The Ca^{2+}-induced clustering of r-n16.3 oligomers requires some degree of protein reorganization.[32−34,47,48] This, in turn, changes the molecular environment around the Trp residues. (b) The Trp residues themselves may be involved in the formation and/or stabilization of r-n16.3 complexes. Hence, Trp residues must reorganize when apo-r-n16.3 complexes shift toward Ca^{2+}-mediated oligomeric clusters. On the basis of bioinformatics predictions (Figure S1, Supporting Information) and NMR data (Figure 2), we believe that scenario b is likely; however, additional experiments involving Trp mutations of the n16.3 sequence would be necessary to affirm these conclusions, and these studies are currently underway.

Finally, we schematically outline our major findings within the context of the framework gel matrix and the early events in the mineralization of the nacre layer (Figure 7).[15−17] In this hypothesis, we draw upon recent studies that demonstrated the ability of synthetic and biological gel phase systems to control mineral dimensions and organization.[15,16,49,50] We propose that members of the n16[9,13,14,18] and homologous nacre framework proteomes[11,12] form gel-like protein phases under mineralization conditions (Figures 5 and 7A). The porous nature of these phases would permit the entrapment or collection of

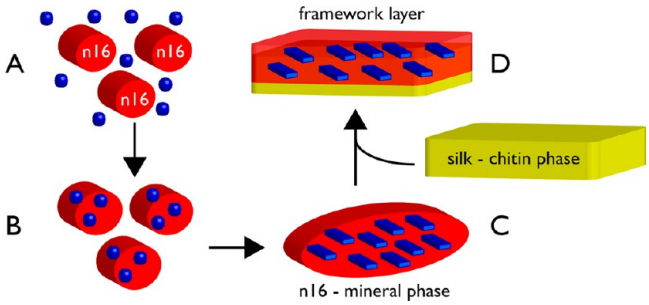

Figure 7. Proposed scheme for n16 proteome phase participation in framework layer nucleation and mineral organization processes. In panel A, the n16 proteome self-associates to form oligomers (red cylinders) during the early phases of nucleation (nanometer-sized mineral deposits, possibly ACC, represented by blue spheres). In panel B, the protein oligomers capture nanomineral deposits and incorporate them into a gel-like environment. Here, the growth of the mineral deposits is now limited by the protein gel. Over time, the protein assemblies unite and create a hybrid protein−mineral phase that now houses numerous single crystals (C, where single crystals are now represented by blue rectangles). At some point, this hybrid phase associates with the silk fibroin−β-chitin gel phase and forms the nacre framework gel layer (D), where further organization and maturation of the entrapped mineral phase are guided by the combined gel phases to create the layered aragonite tablet architecture of the nacre. Note that the shapes and representations utilized in this diagram are arbitrary and not drawn to scale.

dx.doi.org/10.1021/bi401721z | *Biochemistry* 2014, 53, 2739−2748

nanometer-sized forming mineral deposits such as ACC (Figure 7B).[49,50] Once these deposits become associated with this protein gel phase, these mineral particles are now dimensionally limited by the surrounding gel.[49,50] Moreover, depending upon the actual protein concentration, the protein gel phase may also modulate the solubilities of the assembled mineral phases (Table 2 and Figure S3, Supporting Information), which impact postnucleation dissolution and/or reprecipitation or Ostwald ripening processes (Figure 5).[22−28] As demonstrated by our Ca^{2+} experiments (Figure 3), we would expect that these mineral-laden protein complexes would then further associate with each other, forming larger protein phases that house and organize numerous mineral deposits (Figures 5 and 7C). Given that the highly conserved N-terminal sequence of n16 exhibits affinity for silk protein−β-chitin phases,[17] it is likely that the n16 protein phase mineral capture and organization scenario occurs on or within this silk fibroin−β-chitin phase (Figure 7D).[15−17] If true, then the composite framework protein−silk−polysaccharide gel phase would provide a compartmentalized environment for the three-dimensional ordering and eventual maturation of aragonite single crystals, much in the same way that protein assemblies define and direct the pathway for hydroxyapatite crystal maturation and organization in vertebrate tooth enamel.[47,48] We await future studies that can provide insights into the framework protein-guided nucleation and maturation processes of nacre tablet formation.

■ ASSOCIATED CONTENT

Supporting Information

Primary sequence and bioinformatics (Figure S1), AFM imaging of a 70 μM r-n16.3 NMR sample at pH 7.5 (Figure S2), potentiometric curves of ion solubility as a function of assay time (Figure S3), and the methodologies utilized in bioinformatics prediction of intrinsically disordered and amyloid-like aggregation-prone sequences in n16.3. This material is available free of charge via the Internet at http://pubs.acs.org.

■ AUTHOR INFORMATION

Corresponding Author

*Division of Basic Sciences and Craniofacial Biology, New York University, 345 E. 24th St., New York, NY 10010. E-mail: jse1@nyu.edu. Telephone: (212) 998-9605. Fax: (212) 995-4087.

Funding

Research supported by the U.S. Department of Energy, Office of Basic Energy Sciences, Division of Materials Sciences and Engineering, via Grant DE-FG02-03ER46099. H.C. and A.R. thank the Konstanz Research School of Chemical Biology for a Ph.D. stipend for A.R. and financial support.

Notes

The authors declare no competing financial interest.

■ ACKNOWLEDGMENTS

We thank Christopher Ponce for his assistance in the collection of fluorescence spectroscopy data. This report represents contribution 73 from the Laboratory for Chemical Physics, New York University.

■ ABBREVIATIONS

r-n16.3, recombinant nacre framework protein n16.3; CN-n16.3, uniformly labeled ^{13}C, ^{15}N recombinant n16.3; ACC, amorphous calcium carbonate; PNC, prenucleation cluster; ECM, extracellular matrix.

■ REFERENCES

(1) Southgate, P., and Lucas, J. (2008) in *The Pearl Oyster: A Beginner's Guide to Programming Images, Animation, and Interaction*, pp 77−102, Elsevier BV, Oxford, U.K.

(2) Xie, L.-P., Zhu, F.-J., Zhou, Y.-J., Uang, C., and Zhang, R.-Q. (2011) Molecular approaches to understand biomineralization of shell nacreous layer. In *Molecular Biomineralization, Progress in Molecular and Subcellular Biology* (Muller, W. E. G., Ed.) Vol. *52*, pp 331−352, Springer-Verlag, Berlin.

(3) Jäger, C., and Cölfen, H. (2007) Fine structure of nacre revealed by solid-state 13-C and 1-H NMR. *CrystEngComm 9*, 1237−1244.

(4) Nassif, N., Pinna, N., Gehrke, N., Antonetti, M., Jaer, C., and Colfen, H. (2005) Amorphous layer around aragonite platelets in nacre. *Proc. Natl. Acad. Sci. U.S.A. 102*, 12653−12655.

(5) Yan, Z., Ma, Z., Zheng, G., Feng, Q., Wang, H., Xie, L., and Zhang, R. (2008) The inner-shell film: An intermediate structure participating in pearl oyster shell formation. *ChemBioChem 9*, 1093−1099.

(6) Checa, A. G., Cartwright, J. H. E., and Willinger, M. G. (2009) The key role of the surface membrane in why gastropod nacre grows in towers. *Proc. Natl. Acad. Sci. U.S.A. 106*, 38−43.

(7) Falini, G., Albeck, S., Weiner, S., and Addadi, L. (1996) Control of aragonite or calcite polymorphism by mollusk shell macromolecules. *Science 271*, 67−69.

(8) Kinoshita, S., Wang, N., Inoue, H., Maeyama, K., Okamoto, K., Nagai, K., Kondo, H., Hirono, I., Asakawa, S., and Watabe, S. (2011) Deep sequencing of ESTs from nacreous and prismatic layer producing tissues and a screen for novel shell formation-related genes in the pearl oyster. *PLoS One 6*, 1−19.

(9) Marie, B., Joubert, C., Tayale, A., Zanella-Cleon, I., Belliard, C., Piquemal, D., Cochennec-Laureau, N., Marin, F., Gueguen, Y., and Montagnani, C. (2012) Different secretory repertoires control the biomineralization processes of prism and nacre deposition of the pearl oyster shell. *Proc. Natl. Acad. Sci. U.S.A. 109*, 20986−20991.

(10) Nogawa, C., Baba, H., Masaoka, T., Aoki, H., and Samata, T. (2012) Genetic structure and polymorphisms of the N16 gene in *Pinctada fucata*. *Gene 504*, 84−91.

(11) Gardner, L. D., Mills, D., Wiegand, A., Leavesley, D., and Elizur, A. (2011) Spatial analysis of biomineralization associated gene expression from the mantle organ of the pearl oyster, *Pinctada maxima*. *BMC Genomics 12*, 455−470.

(12) Montagnani, C., Marie, B., Marin, F., Belliard, C., Riquet, F., Tayale, A., Zanella-Cleon, I., Fleury, E., Gueguen, Y., Piquemal, D., and Cochennec-Laureau, N. (2011) Pmarg-pearlin is a matrix protein involved in nacre framework formation in the pearl oyster *Pinctada margaritifera*. *ChemBioChem 12*, 2033−2043.

(13) Fang, D., Xu, G., Hu, Y., Pan, C., Xie, L., and Zhang, R. (2011) Identification of genes directly involved in shell formation and their functions in pearl oyster, *Pinctada fucata*. *PLoS One 6*, 1−13.

(14) Zhang, G., et al. (2012) The oyster genome reveals stress adaptation and complexity of shell formation. *Nature 490*, 49−54.

(15) Levi-Kalisman, Y., Falini, G., Addadi, L., and Weiner, S. (2001) Structure of the nacreous organic matrix of a bivalve mollusk shell examined in the hydrated state using cryo-TEM. *J. Struct. Biol. 135*, 8−17.

(16) Nudleman, F., Shimoni, E., Klein, E., Rousseau, M., Bourrat, X., Lopez, E., Addadi, L., and Weiner, S. (2008) Forming nacreous layer of the shells of the bivalves *Atrina rigida* and *Pinctada margaritifera*: An environmental- and cryo-scanning electron microscopy study. *J. Struct. Biol. 162*, 290−300.

(17) Keene, E. C., Evans, J. S., and Estroff, L. A. (2010) Silk fibroin hydrogels coupled with the n16N-β-chitin complex: An in vitro organic matrix for controlling calcium carbonate mineralization. *Cryst. Growth Des. 10*, 5169−5175.

(18) Samata, T., Hayashi, N., Kono, M., Hasegawa, K., Horita, C., and Akera, S. (1999) A new matrix protein family related to the nacreous layer formation of *Pinctada fucata*. *FEBS Lett. 462*, 225−232.
(19) Ponce, C. B., and Evans, J. S. (2011) Polymorph crystal selection by n16, an intrinsically disordered nacre framework protein. *Cryst. Growth Des. 11*, 4690−4696.
(20) Suzuki, M., Saruwatari, K., Kogure, T., Yamamoto, Y., Nishimura, T., Kato, T., and Nagasawa, H. (2009) An acidic matrix protein, Pif, is a key macromolecule for nacre formation. *Science 325*, 1388−1390.
(21) Evans, J. S. (2012) Identification of intrinsically disordered and aggregation: Promoting sequences within the aragonite-associated nacre proteome. *Bioinformatics 28*, 3182−3185.
(22) Gebauer, D., Volkel, A., and Coelfen, H. (2008) Stable prenucleation of calcium carbonate clusters. *Science 322*, 1819−1822.
(23) Gebauer, D., and Cölfen, H. (2011) Prenucleation clusters and non-classical nucleation. *Nano Today 6*, 564−584.
(24) Demichelis, R., Raiteri, P., Gale, J. D., Quigley, D., and Gebauer, D. (2011) Stable prenucleation mineral clusters are liquid-like polymers. *Nat. Commun. 2*, 1−8.
(25) Gebauer, D., Cölfen, H., Verch, A., and Antonietti, M. (2008) The multiple roles of additives in $CaCO_3$ crystallization: A quantitative case study. *Adv. Mater. 21*, 435−439.
(26) Verch, A., Gebauer, D., Antonietti, M., and Cölfen, H. (2011) How to control the scaling of $CaCO_3$: A "fingerprinting technique" to classify additives. *Phys. Chem. Chem. Phys. 13*, 16811−16820.
(27) Stephens, C. J., Kim, Y. Y., Evans, S. D., Meldrum, F. C., and Christenson, H. K. (2011) Early stages of crystallization of calcium carbonate revealed in picoliter droplets. *J. Am. Chem. Soc. 133*, 5210−5213.
(28) Stephens, C. J., Ladden, S. F., Meldrum, F. C., and Christenson, H. K. (2010) Amorphous calcium carbonate is stabilized in confinement. *Adv. Mater. 20*, 2108−2115.
(29) Perovic, I., Mandal, T., and Evans, J. S. (2013) A pearl protein self-assembles to form protein complexes that amplify mineralization. *Biochemistry 52*, 5696−5703.
(30) Nečas, D., and Klapetek, P. (2012) Gwyddion: An open-source software for SPM data analysis. *Cent. Eur. J. Phys. 10*, 181−188.
(31) Wang, Y., and Wishart, D. S. (2005) A simple method to adjust inconsistently referenced 13-C and 15-N chemical shift assignments of proteins. *J. Biomol. NMR 31*, 143−148.
(32) Bromley, K. M., Kiss, A. S., Lokappa, S. B., Lakshminarayanan, R., Fan, D., Ndao, M., Evans, J. S., and Moradian-Oldak, J. (2011) Dissecting amelogenin nanospheres: Characterization of metastable oligomers. *J. Biol. Chem. 286*, 34643−34653.
(33) Vivian, J. T., and Callis, P. R. (2001) Mechanisms of tryptophan fluorescence shifts in proteins. *Biophys. J. 80*, 2093−2091.
(34) Chen, Y., and Barkley, M. D. (1998) Towards understanding tryptophan fluorescence in proteins. *Biochemistry 37*, 9976−9982.
(35) Delak, K., Harcup, C., Lakshminarayanan, R., Zhi, S., Fan, Y., Moradian-Oldak, J., and Evans, J. S. (2009) The tooth enamel protein, porcine amelogenin, is an intrinsically disordered protein with an extended molecular configuration in the monomeric form. *Biochemistry 48*, 2272−2281.
(36) Ndao, M., Dutta, K., Bromley, K., Sun, Z., Lakshminarayanan, R., Rewari, G., Moradian-Oldak, J., and Evans, J. S. (2011) Probing the self-association, intermolecular contacts, and folding propensity of amelogenin. *Protein Sci. 20*, 724−734.
(37) Ndao, M., Ponce, C. B., and Evans, J. S. (2012) Oligomer formation, metalation, and the existence of aggregation-prone and mobile sequences within the intracrystalline protein family, Asprich. *Faraday Discuss. 159*, 449−462.
(38) Uversky, V. N. (2002) Natively unfolded proteins: A point where biology waits for physics. *Protein Sci. 11*, 739−756.
(39) Tompa, P. (2002) Intrinsically unstructured proteins. *Trends Biochem. Sci. 27*, 527−533.
(40) Meng, J., Romero, P., Yang, J. Y., Chen, J. W., Vacic, V., Obradovic, Z., and Uversky, V. N. (2008) The unfoldomics decade: An update on intrinsically disordered proteins. *BMC Genomics 9*, 1−26.
(41) Peysselon, F., Xue, B., Uversky, V. N., and Ricard-Blum, S. (2011) Intrinsic disorder of the extracellular matrix. *Mol. BioSyst. 7*, 3353−3365.
(42) Rao, A., Berg, J. K., Kellermeier, M., and Gebauer, D. (2013) Sweet on biomineralization: Effect of carbohydrates on the early stages of calcium carbonate crystallization. *European Journal of Mineralization*, DOI: 10.1127/0935-1221/2014/0026-2379.
(43) Amos, F. F., Ndao, M., Ponce, C. B., and Evans, J. S. (2011) A C-RING-like domain participates in protein self-assembly and mineral nucleation. *Biochemistry 50*, 8880−8887.
(44) Michenfelder, M., Fu, G., Lawrence, C., Weaver, J. C., Wustman, B. A., Taranto, L., and Evans, J. S. (2003) Characterization of two molluscan crystal-modulating biomineralization proteins and identification of putative mineral binding domains. *Biopolymers 70*, 522−533.
(45) Zhang, G., and Xu, J. (2013) From colloidal nanoparticles to a single crystal: New insights in the formation of nacre's aragonite tablets. *J. Struct. Biol. 182*, 36−43.
(46) Sato, A., Nagasaka, S., Furihata, K., Nagata, S., Arai, I., Saruwatari, K., Kogure, T., Sakuda, S., and Nagasawa, H. (2011) Glycolytic intermediates induce amorphous calcium carbonate formation in crustaceans. *Nat. Chem. Biol. 7*, 197−199.
(47) Chandrababu, K. B., Dutta, K., Lokappa, S. B., Ndao, M., Evans, J. S., and Moradian-Oldak, J. (2014) Structural adaptation of tooth enamel protein amelogenin in the presence of SDS micelles. *Biopolymers 101*, 525−535.
(48) Bromley, K. M., Kiss, A. S., Lokappa, S. B., Lakshminarayanan, R., Fan, D., Ndao, M., Evans, J. S., and Moradian-Oldak, J. (2011) Dissecting amelogenin nanospheres: Characterization of metastable oligomers. *J. Biol. Chem. 286*, 34643−34653.
(49) Addadi, L., Joester, D., Nudleman, F., and Weiner, S. (2006) Mollusk shell formation: A source of new concepts for understanding biomineralization processes. *Chem.—Eur. J. 12*, 980−987.
(50) Gal, A., Habraken, W., Gur, D., Fratzl, P., Weiner, S., and Addadi, L. (2013) Calcite crystal growth by a solid-state transformation of stabilized amorphous calcium carbonate nanospheres in a hydrogel. *Angew. Chem., Int. Ed. 52*, 4867−4870.